Parameter Optimization for Vibratory Harvesting of Wolfberry Branches Based on Dual Low-Frequency Vibration Excitation and Singular Value Spectrum

Guangrui Hu [a,†] Shilong Feng,[b,†] Qianwen Kou,[b] Shuling Zhang [b] Yun Chen,[b] Lizhu Jin [b] Teng Zhang,[b] Li Zhao,[b] and Lingxin Bu [b,*]

To overcome empirical and discrete parameter selection and severe energy attenuation in wolfberry (*Lycium barbarum* L.) harvesting using single-source vibration, in this study, a dual-source low-frequency excitation method is proposed. Using 'Ningqi No.7' branches and a two-point synchronous excitation device, the effects of the amplitude (28 to 80 mm) and phase (-180° to 180°) of the upper and lower vibration sources (UVS and LVS) on the detachment percentages of the middle section, lower section, and the total detachment (TD) were investigated *via* response surface methodology. Singular value spectrum analysis of the acceleration signals extracted the maximum singular value (MSV) to quantify the overall branch vibration energy. Two main low-frequency modes near 4 Hz and 8 Hz with high damping were identified. The MSV was strongly correlated with TD (r = 0.751), confirming its reliability for effectiveness evaluation. The optimal parameters found were a UVS of 80 mm, LVS of 68 mm, and phase of 135°, yielding a TD of 85.9% in validation. This demonstrates that the synergistic control of amplitude and phase at a low frequency enhances the harvest efficiency, offering a new approach for intelligent parameter optimization based on vibration monitoring.

DOI: 10.15376/biores.21.2.3931-3953

Keywords: Lycium barbarum L.; Vibrating harvest; Parameter experiment; Singular value decomposition; Response surface methodology

Contact information: a: *School of Design, Xi'an Technological University, Xi'an; b: College of Mechatronic Engineering, North Minzu University, Yinchuan;*
** Corresponding author: 2021023@nmu.edu.cn;*
†*These authors contributed equally to this work and should be considered co-first authors.*

INTRODUCTION

Wolfberries (*Lycium barbarum* L.) are recognized worldwide as a functional food with medicinal and nutritional properties. According to the *Report on the High-Quality Development of China's Modern Wolfberry Industry* (2024), China's total fresh wolfberry production reached 1.40 million tons in 2023, and dried wolfberry production amounted to 240,000 tons. Export revenue reached RMB 750 million, representing a year-on-year increase of 23.1% compared to 2022. Gansu, Qinghai, Ningxia, and Xinjiang Provinces account for more than 98% of the wolfberry planting area in China. In major wolfberry-producing counties, approximately 50% of farmers' average operating income is derived from wolfberries. Thus, this industry is both a characteristic and advantageous sector in northwestern China. It is of significant importance for regional industrial structure

optimization and income growth among farmers and herders. Wolfberries are predominantly harvested manually, which is highly labor-intensive. Harvesting labor accounts for more than 50% of the total labor input in wolfberry production (Li *et al.* 2024) and harvesting costs exceed 40% of the total labor cost (Chen *et al.* 2025a). Consequently, the development of mechanized harvesting technologies has become an urgent need in the wolfberry industry.

Wolfberry harvesting device types include comb-brush, pneumatic, brush–vibration, and vibratory. Handheld comb-brush harvesters have low efficiency and impose a labor intensity comparable to that of manual harvesting (Jiang *et al.* 2024). Pneumatic harvesters require high energy consumption (Chen *et al.* 2021). Brush–vibration harvesters, in which rubber rollers simultaneously rotate and reciprocate vertically to strike wolfberry branches, cause direct impact damage to the fruit (Zhao *et al*. 2021a). Vibratory harvesting devices have attracted increasing attention because of their simple structure and high operational efficiency. Table 1 summarizes the key parameters and harvesting performance of recently developed vibratory wolfberry harvesters. Previous studies have focused on the picking and damage percentages of ripe fruit and the detachment percentage of unripe fruit. However, the selection of critical excitation parameters, such as the vibration frequency (2.5 to 48 Hz) and amplitude (15 to 70 mm), relies heavily on researchers' experience, resulting in substantial discrepancies across studies. Although increasing the vibration frequency and amplitude facilitate the fruit detachment to some extent, it also leads to higher percentages of unripe fruit detachment, increased damage to ripe fruit, and a greater risk of plant structural damage (Deng *et al*. 2026).

Table 1. Research Status of Selected Vibratory Wolfberry Harvesting Devices

Reference	Vibration Source Mechanism	Vibration Frequency (Hz)	Vibration Amplitude (mm)	Detachment Percent of Ripe Fruit (%)	Detachment Percent of Unripe Fruit (%)	Damage Percent of Ripe Fruit (%)
Zhang *et al.* 2015	Offset disc	48	-	86.70	7.36	8.62
Zhang *et al.* 2018	Crank–slider	12	40	90.52	5.72	2.54
Mei *et al.* 2019	Crank–slider	37.5	40	96.40	-	3.40
Peng *et al.* 2019	Crank–slider	17	30	94.40	-	2.74
Wan *et al.* 2021	Offset disc	2.5	70	91.23	3.14	1.85
Mei *et al.* 2024	Crank–slider	21.67	15	88.95	3.80	3.64
Chen *et al.* 2024a	Offset disc	9	44	86.44	6.81	5.54
Chen *et al.* 2024b	Offset disc	19.12	-	95.67	4.68	3.70
Chen *et al.* 2025b	Crank–slider	7.5	50	82.69	3.13	4.06
Wei *et al.* 2025	Offset disc	9	-	85.40	4.61	3.19

To better match the excitation parameters with plant characteristics, previous studies have primarily employed single-source excitation to determine the mechanical properties of wolfberry plants, focusing on their natural frequencies and energy transmission behavior. Zhao *et al.* (2021) developed a finite element model for wolfberries based on a transversely isotropic constitutive model. Modal analysis has been conducted to determine the natural frequencies of different modes, and experimental modal testing using accelerometers and an impact hammer have been performed to identify the resonance frequencies of wolfberries. However, variations in plant architecture and the simplifications introduced during model construction significantly affect the accuracy of modal analysis results (Macoretta *et al.* 2025). He *et al.* (2018) investigated the acceleration responses of fruit-bearing branches when excitation was applied at different locations on the plant. They showed that acceleration attenuation from primary third-order branches to fruit-bearing branches was approximately five-fold, and that attenuation from lateral third-order branches to fruit-bearing branches reached nearly six-fold. Wang *et al.* (2018) analyzed the relative motion between wolfberry fruit and branches during the detachment process using high-speed photography and revealed that fruit on the same fruit-bearing branch detached in different sequences, with fruit located closer to the vibration source detaching earlier. These studies collectively indicate that wolfberries undergo forced vibration under external excitation, and that energy transmission along branches is strongly influenced by internal damping and external factors, such as flowers, leaves, and fruit. As a result, excitation forces experience severe attenuation along the branch, making it difficult for vibrational energy to effectively propagate to distal regions, which leads to poor fruit detachment at locations far from the vibration source (Sola-Guirado *et al.* 2022).

Given the risk of plant damage associated with excessively high vibration frequencies and the inefficiency of fruit detachment under single-source excitation (Deng *et al.* 2025), prolonged operation of vibratory harvesting devices has been reported to induce numbness in the upper limbs of operators (Zhao *et al*. 2021b). Vibration exposure has been demonstrated to cause temporary alterations in vibrotactile sensitivity (Morioka and Griffin 2002). Specifically, exposure to vibration at 31.5 Hz and above for 32 min results in a temporary threshold shift (TTS) in the vibration perception threshold (VPT), accompanied by paresthesia and numbness (Malchaire *et al*. 1998). Therefore, it is essential to reduce the vibration frequency and limit the continuous working duration of operators. This study proposes the hypothesis: for wolfberry branches excited at a fixed low frequency (near the first-order natural frequency), the simultaneous application of two vibration sources with controlled amplitudes and phase relationships can create a superimposed vibration state that enhances the overall branch vibration energy and consequently improves the fruit detachment percentage, compared to single-source excitation at the same frequency. To test this hypothesis, this study explored the application of dual-source excitation to wolfberry branches. The specific objectives of this study were to: (1) characterize the low-frequency vibration modes and damping properties of wolfberry branches using singular value spectrum analysis; (2) investigate the effects of the amplitudes of the two vibration sources and their phase relationship on ripe fruit detachment percentages through response surface methodology; and (3) establish a quantitative correlation between the maximum singular value (MSV) extracted from the acceleration signals and the fruit detachment percentage, thereby evaluating the feasibility of using MSV as a vibration-state indicator for parameter optimization.

EXPERIMENTAL METHODS

Fresh Samples and Experimental Device

Field experiments were conducted from October 1 to 4, 2025, on wolfberry cultivar 'Ningqi No. 7' in an orchard located in Baiqiao Village, Zhongwei City, Ningxia Hui Autonomous Region, China (105.20° E, 37.56° N). Figure 1 shows the structure of the experimental apparatus. The linear motion module was equipped with two movable platforms, each mounting a crank–slider mechanism driven by a DC motor (DC 24 V, frequency range 0 to 4 Hz), which served as the upper and lower vibration sources (UVS and LVS). Branches bearing a relatively large amount of fruit were selected from orchard plants, cut, and fixed at the cut end to the experimental device so that the branch could hang freely under natural gravity. The heights of the two crank–slider mechanisms were adjusted to positions corresponding to the upper and lower one-third of the total branch length. The branch was secured to the ends of the crank–slider mechanisms using cable ties. Thus, the branch was divided into upper, middle, and lower sections, and the number of fruits in each section was recorded before and after the experiment. As the upper section contained few fruits, dynamic accelerometers were installed at the midpoints of the middle and lower sections of the branch. Acceleration signals were acquired and processed using a COCO-90 dynamic signal analyzer (Crystal Instruments Co., Ltd., Santa Clara, CA, USA). Branch morphological parameters, including the branch diameters at the vibration source fixation points (P_{d1} and P_{d2}), branch diameters at the upper and lower endpoints (P_{s1} and P_{s2}, denoted as D_{d1}, D_{d2}, D_{s1}, and D_{s2}), and the total branch length (L) were recorded as characteristic descriptors.

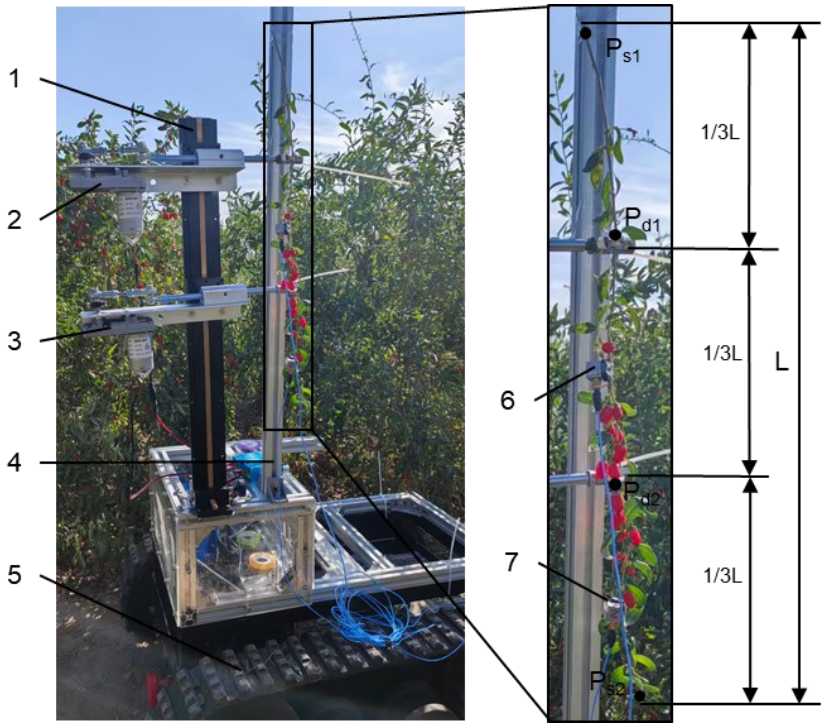

Fig. 1. Overview of the test device: (1) linear motion module, (2) upper vibration source (UVS); (3) lower vibration source (LVS), (4) base frame, (5) mobile platform, (6) upper acceleration sensor (UAS), and (7) lower acceleration sensor (LAS)

Experimental Design

In preliminary experiments, fruit detachment was evaluated under conditions in which both vibration sources operated at the maximum amplitude of 80 mm and frequencies of 1, 2, 3, and 3.5 Hz. The fruit detachment percentage remained below 20% at all of these frequencies. In contrast, fruit detachment increased when the excitation frequency increased to 4 Hz. This improvement is likely attributable to the proximity of 4 Hz to the natural frequency of wolfberry branches (Su *et al*. 2025). Thus, the excitation frequencies of both vibration sources were fixed at 4 Hz in subsequent experiments. It should be noted that 4 Hz was the upper operational frequency limit of the DC motor (DC 24 V) used in this study, which physically constrained the frequency range that could be explored. The UVS and LVS employed identical crank–slider mechanisms, as illustrated in Fig. 2(a). The lengths of connecting rod 2 and reciprocating rod 3 (L_2 and L_3) were 85 mm and 235 mm, respectively. The length of crank 1 (L_1) could be adjusted within 14 to 40 mm by changing the position of joint 1, resulting in a displacement amplitude of 28 to 80 mm for the reciprocating rod. In addition, the excitation phase relationship between the UVS and LVS was considered, as it could alter the vibration state of the branch and thereby influence fruit detachment. Three phase conditions, namely 180°, 0°, and −180°, were established, as shown in Figs. 2(b), (c), and (d), respectively.

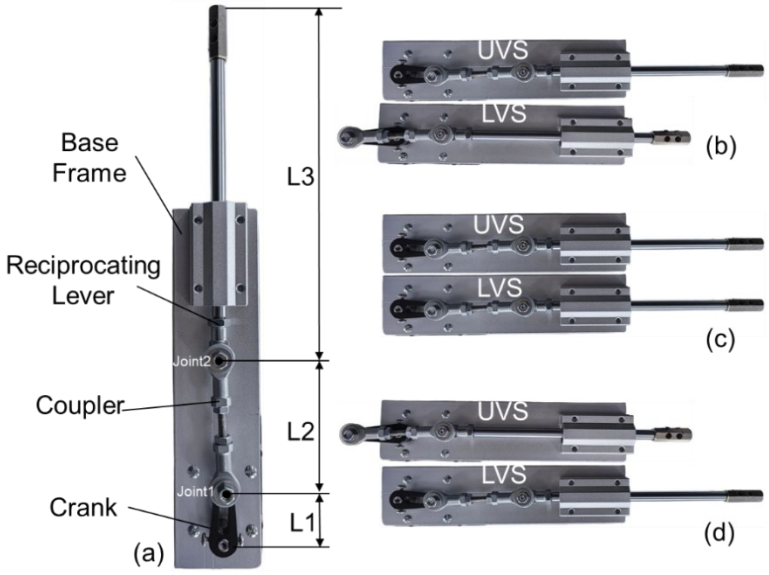

Fig. 2. Structure of the vibratory excitation device and phase configurations of the upper and lower vibration sources during the experiment

Using Design-Expert software V13, a three-factor, three-level Box-Behnken design was developed with the amplitudes of the UVS and LVS and the excitation phase as the independent variables. A quadratic regression response surface methodology (RSM) was applied to determine the responses of the fruit detachment percentage in the middle (DPM, Y_1) and lower parts of the branches (DPL, Y_2), and the total fruit detachment percentage (TD, Y_3) to the experimental factors.

Each experimental condition was repeated five times. Each vibration test lasted 10 s. The total number of ripe fruits in the middle (N_1) and lower parts of the branch (N_2) were recorded before each test, and the remaining number of ripe fruits in the middle (n_1) and

lower parts (n_2) were recorded after the test. The fruit detachment percentages were calculated using Eqs. 1 to 3:

$$Y_1 = \frac{\sum(N_{1i} - n_{1i})}{\sum N_{1i}}, \quad (1)$$

$$Y_2 = \frac{\sum(N_{2i} - n_{2i})}{\sum N_{2i}}, \quad (2)$$

$$Y_3 = \frac{\sum(N_{1i} + N_{2i} - n_{1i} - n_{2i})}{\sum(N_{1i} + N_{2i})}, \quad (3)$$

where i denotes the replicate number within each experimental condition, and i = 1 to 5.

The response variables were fitted using a general quadratic polynomial model, expressed in Eq. 4 (Bu *et al.* 2020). Table 2 presents coded levels of the experimental factors.

$$Y = \beta_0 + \sum_{i=1}^{3} \beta_i X_i + \sum_{i=1}^{3} \beta_{ii} X_i^2 + \sum_{i=1}^{2} \sum_{j=i+1}^{3} \beta_{ij} X_i X_j, \quad (4)$$

where Y is the response variable measured for each combination of factors; and β_0, β_i, β_{ii}, and β_{ij} are terms of regression coefficients for intercept, linearity, square, and interaction, respectively.

Table 2. Factor Codes of the Independent Variable Levels

Factors	Unit	−1	0	1
Amplitude of UVS (X_1)	mm	28	54	80
Amplitude of LVS (X_2)	mm	28	54	80
Excitation phase (X_3)	°	−180	0	180

Acceleration Signal Processing and Singular Value Spectrum Calculation

Acceleration signals recorded by the upper and lower accelerometers (UAS and LAS, respectively) were used to compute singular value spectra under different experimental conditions, providing a quantitative representation of branch vibration states. Singular value decomposition (SVD) is based on energy with the characteristic that useful signal singular values are significantly larger than noise singular values, which makes it suitable for vibration signal denoising (Liu *et al.* 2017). SVD is commonly employed in engineering applications for identifying natural frequencies, ranking modal energy contributions, and estimating system damping (Miao *et al.* 2015). In the COCO-90 vibration signal analyzer, a Hanning window was applied to the time-domain acceleration responses of the wolfberry branches to suppress spectral leakage. The signals from different channels were superimposed using Post Analyzer software (Version: 2016) to enhance the strength of the effective signals. The processed signals were truncated to remove invalid data, such as noise at the beginning and end of the signals and abnormal interference segments, retaining only valid vibration response data. Non-stationary signals were denoised using wavelet processing in MATLAB 2023. This approach removed noise components (*e.g.*, hardware noise, environmental interference) and preserved key features of the vibration signal, including natural frequencies, damping, and time/frequency-domain

characteristics related to modal shapes. After multiple practical validations and a comparison of reconstructed signals at different decomposition levels, a decomposition level of five was selected for analysis, as shown in Fig. 3.

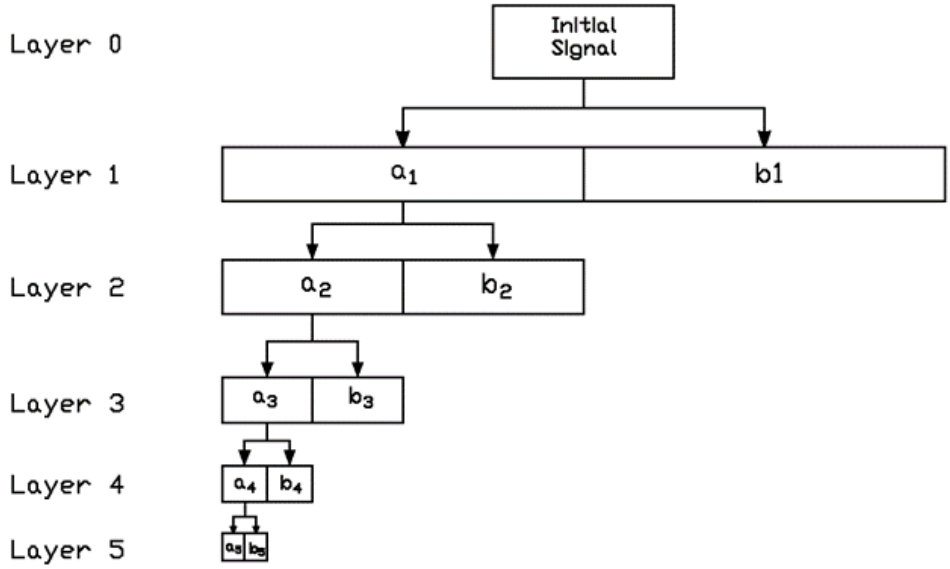

Fig. 3. Signal decomposition process

In the wavelet-based de-noising procedure, the bior3.5 biorthogonal wavelet was selected to maximize the fidelity of the denoised signal to the original time-domain waveform and to preserve the physical characteristics of branch vibration. This selection enabled accurate decomposition and reconstruction of the vibration waveform and retained signal details, particularly for analyses of time-domain decay features, such as damping ratio estimation and modal identification of wolfberry branches. The branch vibration signal was decomposed into low-frequency coefficients, which represent the main vibrational components (*e.g.*, waveforms corresponding to natural frequencies), and high-frequency coefficients, which contain noise (*e.g.*, wind, electronic interference) and local branch features. Soft-threshold function $S_{Th}(Z_K)$ was defined. Threshold $T_h > 0$ was applied to the wavelet coefficients, such that coefficients with absolute values smaller than T_h were set to zero and coefficients with absolute values larger than Th ($|Z_K| > T_h$) were processed according to Eq. 5:

$$Z_K = S_{Th}(Z_K) = \begin{cases} Z_K - T_h, & Z_K \geq T_h \\ 0, & -T_h < Z_K < T_h \\ Z_K + T_h, & Z_K \leq T_h \end{cases} \quad (5)$$

The threshold was determined using the following approach,

$$T_h = \sigma\sqrt{2\ln(N)} \quad (6)$$

where N is the signal length and σ is the standard deviation of the noise, estimated as σ = MAD(b_1) / 0.6745 with MAD representing the median absolute deviation. Specifically, the median of b_1 was computed, and the absolute deviations of each element in $b1$ were then calculated from this median to form a new list. The median of this new list was the MAD value.

Using soft-threshold function $S_{Th}(Z_K)$, the high-frequency coefficients—where noise was primarily concentrated—were either set to zero or shrunk, and the coefficients corresponding to valid signal components were retained. In the high-frequency coefficients of wolfberry branch vibrations, noise appeared as small, irregular-amplitude coefficients, and local branch vibrations exhibited larger, regular-amplitude coefficients. The soft-threshold function effectively removed small-amplitude noise coefficients and preserved significant feature coefficients, achieving smooth shrinkage of coefficients and producing a denoised signal that more accurately reflected the actual branch vibration waveform. Low-frequency coefficients were retained unchanged, and an inverse wavelet transform was applied to reconstruct a clean signal with the noise removed. Covariance-driven frequency-domain modal analysis was then conducted. The acceleration responses from the upper and lower accelerometers were combined into an information matrix, and their cross-power spectral density matrix was computed, capturing amplitude and phase relationships (covariance information) between the two sensors. SVD was applied to this cross-power spectral density matrix at each frequency point to obtain the singular value spectrum (Klema and Laub 1980).

Table 3. Core Parameters for Singular Value Spectrum Calculation

Mathematical Notation	Physical Meaning	Calculation Method and Explanation
N_w	Window length	min ([L_s / 4],1024)
$N_{overlap}$	Number of overlapping points	[N_w×0.5](50% overlap – improves the accuracy of spectral estimation)
N_{fft}	FFT points	$2^{[\log_2 N_w]}$ (the smallest power of 2 ≥ the window length)
N_f	Total number of positive frequency points	N_{fft} / 2 + 1
f_m	m-th frequency point	$f_m = \frac{F_S/2}{N_f - 1} \times (m-1)$, m = 1,2,…, N_f
K	Number of signal segments	$K = \left[\frac{L_s - N_{overlap}}{N_W - N_{overlap}} \right]$
U	Window function normalization factor	$U = \sum_{n=1}^{N_w} w^2(n)$
G_{yy}	Frequency-domain covariance matrix (positive semi-definite, PSD matrix)	2 × 2 × N_f complex matrix − Gyy(i,j,m) represents the cross-power spectral density between the i-th and j-th channels at m-th frequency point f_m
$X_{i,k}(f_m)$	Frequency-domain complex value	Complex value of the k-th signal segment at the i-th channel and frequency point f_m
$P_{ij}(f_m)$	Cross-power spectral density	$P_{ij}(f_m) = P^*_{ij}(f_m)$, $i \neq j$
U_m	2 × 2 unitary matrix	Its column vectors are the orthogonal eigenvectors of $H_m H_m^H$
$\sum_m$	2 × 2 diagonal matrix	Singular values – diagonal elements σ_{m1} and σ_{m2} of the diagonal matrix, satisfying $\sigma_{m1} \geq \sigma_{m2} \geq 0$
V_m^H	Conjugate transpose of the V_m matrix	Column vectors of $H_m H_m^H$, representing the orthogonal eigenvectors of the matrix

The time-domain acceleration signals of wolfberry branches measured by the UAS and LAS were denoted as $x_1(t)$ and $x_2(t)$, respectively, with sampling frequency F_s and total number of samples L_s. Table 3 summarizes the core parameters used in the analysis are (Wall *et al*. 2003). The preprocessed signals were segmented with a 50% window overlap to ensure smoother spectral continuity between adjacent frames. Each segment was windowed individually, and a discrete Fourier transform was used to obtain the frequency-domain complex values:

$$X_{i,k}(f_m) = \sum_{n=0}^{N_{fft}-1} x_{i,k}(n)\, \mathrm{e}^{-j2\pi \frac{mn}{N_{fft}}} \tag{7}$$

The frequency-domain values of the K segments were averaged and normalized to obtain the cross-power spectral density at frequency f_m. The positive semi-definite (PSD) matrix was computed according to Eq. 8,

$$G_{yy} = P_{ij}(f_m) = \frac{1}{KU} \sum_{k=1}^{K} X_{i,k}(f_m) \cdot X_{j,k}^{*}(f_m) \tag{8}$$

where X^* denotes the complex conjugate.

For m-th frequency point f_m, a 2 × 2 complex covariance matrix corresponding to this single frequency point was extracted from the PSD matrix, denoted as follows:

$$H_m = \begin{bmatrix} P_{11}(f_m) & P_{12}(f_m) \\ P_{21}(f_m) & P_{22}(f_m) \end{bmatrix} \tag{9}$$

Due to numerical computation errors, H_m may not satisfy the Hermitian symmetry requirement, $H_m^H = H_m$; that is, H^H is the conjugate transpose. Therefore, a correction must be applied:

$$H_m = \frac{1}{2}\left(H_m + H_m^H\right) \tag{10}$$

SVD was then performed on the corrected 2 × 2 complex matrix H_m:

$$H_m = U_m \cdot \sum\nolimits_m \cdot V_m^H \tag{11}$$

After decomposition, elements σ_{m1} and σ_{m2} on the diagonal of the diagonal matrix correspond to the first and second singular values, respectively. The singular values across the entire frequency range were obtained by repeating this procedure.

RESULTS AND DISCUSSION

Data Statistics

Based on the experimental design in Design-Expert 13, 17 experimental settings were evaluated, each with five replicates. Y_1, Y_2, and Y_3 were calculated based on the total number of fruits in the middle and lower sections before the test and the number of fruits remaining after the test. The MSV of each test was calculated based on the acceleration data recorded by the sensors.

Table 4. Statistical Summary of the Experimental Results

	X_1	X_2	X_3	Y_1	Y_2	Y_3	Test Sequence Number	MSV	N_1	n_1	N_2	n_2	L (mm)	D_{s1} (mm)	D_{d1} (mm)	D_{d2} (mm)	D_{s2} (mm)
1	−1	−1	0	0.00	0.00	0.00	1-1	0.74	14	14	2	2	420	2.32	1.60	1.08	0.62
							1-2	0.78	12	12	5	5	410	2.68	2.40	2.00	1.12
							1-3	0.70	7	7	7	7	390	2.54	2.02	1.48	1.00
							1-4	0.68	12	12	5	5	420	1.88	1.60	1.20	0.40
							1-5	0.46	6	6	6	6	410	1.86	1.74	1.42	0.54
2	0	0	0	0.57	0.65	0.59	2-1	1.25	19	4	6	1	475	2.56	2.12	1.42	0.96
							2-2	1.31	14	10	2	0	540	3.62	2.68	1.92	0.70
							2-3	1.48	6	2	6	2	540	2.34	1.82	1.66	0.76
							2-4	1.44	5	3	7	5	480	1.88	1.68	1.48	0.50
							2-5	1.35	12	5	2	0	450	2.94	2.60	2.22	1.12
3	0	0	0	0.44	0.74	0.56	3-1	0.91	9	5	6	4	530	2.84	2.48	1.60	0.72
							3-2	1.39	12	8	3	0	560	3.50	3.20	2.44	1.54
							3-3	1.46	2	1	8	1	510	2.50	2.32	1.78	0.80
							3-4	1.36	6	3	9	2	400	2.38	2.00	1.10	0.62
							3-5	1.32	14	7	1	0	510	2.62	2.54	2.00	0.80
4	0	0	0	0.54	0.69	0.60	4-1	1.46	8	4	5	0	370	2.20	1.72	1.20	0.52
							4-2	1.35	14	6	3	2	530	2.42	1.78	1.62	0.60
							4-3	1.30	2	1	7	2	390	2.02	1.78	1.54	0.72
							4-4	1.42	4	1	5	1	490	2.12	1.60	1.14	0.72
							4-5	1.52	11	6	6	3	550	3.40	2.98	2.32	1.28
5	−1	0	−1	0.08	0.23	0.16	5-1	1.01	3	1	13	7	440	3.00	2.60	2.22	1.14
							5-2	0.89	10	10	1	0	470	2.98	2.08	1.64	0.74
							5-3	0.82	5	5	19	17	580	2.60	2.12	1.48	0.78
							5-4	0.86	6	5	3	3	510	2.50	2.12	1.60	0.54
							5-5	0.97	14	14	3	3	500	2.92	2.42	1.82	0.80
6	1	0	−1	0.73	0.73	0.73	6-1	2.31	4	1	11	4	550	2.40	2.22	1.52	0.90
							6-2	2.23	15	3	14	9	550	3.30	2.78	1.70	0.70

							6-3	2.01	4	0	15	1	400	2.20	1.74	1.20	0.34
							6-4	1.56	7	2	7	0	390	2.54	2.02	1.48	1.00
							6-5	1.35	11	5	5	0	630	3.70	2.96	2.30	0.76
7	1	1	0	0.75	0.74	0.75	7-1	2.37	12	4	11	6	500	2.70	2.20	1.56	0.70
							7-2	1.84	11	5	6	4	470	2.68	2.40	2.00	1.12
							7-3	2.58	4	1	8	0	500	2.78	2.36	1.60	0.60
							7-4	2.32	10	0	7	0	490	2.74	2.60	1.82	0.72
							7-5	2.05	19	4	7	0	600	3.64	3.00	1.98	0.84
8	−1	1	0	0.30	0.62	0.47	8-1	1.19	7	5	11	6	415	2.54	2.14	1.50	0.60
							8-2	1.09	8	4	9	0	470	1.88	1.60	1.32	0.70
							8-3	1.06	5	4	10	4	410	2.52	2.08	1.52	0.80
							8-4	0.91	11	8	4	2	430	2.34	2.00	1.58	0.70
							8-5	1.20	9	7	11	5	560	3.40	3.22	2.40	1.00
9	0	0	0	0.43	0.58	0.52	9-1	1.52	5	1	15	5	420	2.14	2.04	1.62	0.72
							9-2	1.43	19	12	4	4	690	4.30	3.78	2.26	0.86
							9-3	1.36	4	2	16	5	430	2.08	1.74	1.32	0.62
							9-4	1.37	4	2	8	0	480	2.22	2.00	1.12	0.56
							9-5	1.43	10	7	10	8	510	3.48	2.88	2.22	1.34
10	−1	0	1	0.22	0.31	0.27	10-1	0.91	10	9	12	7	420	2.48	1.92	1.50	0.64
							10-2	0.95	13	8	3	1	400	2.60	2.20	1.58	0.90
							10-3	0.94	6	5	20	19	580	2.60	2.12	1.48	0.78
							10-4	0.81	5	3	3	2	510	2.50	2.12	1.60	0.54
							10-5	1.16	11	10	7	2	500	3.00	2.28	1.58	0.74
11	0	−1	1	0.26	0.13	0.20	11-1	0.73	7	3	14	12	510	2.40	2.00	1.62	0.60
							11-2	0.95	12	8	3	2	550	3.24	2.62	1.78	0.80
							11-3	0.98	9	7	12	11	390	2.50	2.08	1.20	0.70
							11-4	1.06	6	5	7	7	480	1.88	1.68	1.48	0.50
							11-5	0.97	24	20	4	3	540	3.00	2.82	2.16	0.70
12	1	−1	0	0.80	0.69	0.75	12-1	1.96	9	4	5	1	420	2.22	2.00	1.48	0.60
							12-2	2.25	9	2	7	5	590	2.40	2.00	1.64	0.54

							12-3	2.07	10	2	13	2	430	2.42	2.32	1.38	0.72
							12-4	2.26	4	0	10	4	370	2.46	2.34	1.30	0.60
							12-5	2.23	17	2	4	0	460	2.30	2.00	1.20	0.62
13	0	1	1	0.70	0.72	0.71	13-1	2.18	13	3	6	3	400	2.22	1.74	1.48	0.60
							13-2	2.14	10	5	18	9	540	3.10	2.22	1.72	0.70
							13-3	2.15	2	0	5	0	500	2.42	1.92	1.24	0.72
							13-4	2.02	2	1	13	1	410	2.32	2.08	1.32	0.74
							13-5	2.10	13	3	8	1	590	2.90	2.00	1.40	0.64
14	0	1	−1	0.34	0.79	0.51	14-1	2.19	12	9	6	3	410	2.18	1.82	1.30	0.64
							14-2	2.15	12	8	3	0	400	2.50	2.08	1.50	0.56
							14-3	2.08	16	11	5	0	560	3.08	2.46	1.62	0.80
							14-4	2.10	1	0	15	3	470	2.38	1.88	1.62	0.78
							14-5	2.11	15	9	4	1	550	3.38	2.52	1.90	0.60
15	1	0	1	0.92	0.79	0.86	15-1	2.46	5	0	10	0	450	2.04	1.78	1.48	0.42
							15-2	2.37	5	0	11	5	500	3.00	2.42	1.70	0.58
							15-3	2.37	5	1	8	1	420	1.92	1.70	1.60	0.78
							15-4	2.39	14	2	4	1	480	2.70	2.30	1.52	0.72
							15-5	2.26	7	0	1	0	580	2.70	2.30	1.52	0.72
16	0	−1	−1	0.22	0.10	0.17	16-1	1.34	14	12	8	6	420	2.22	1.68	1.10	0.64
							16-2	0.97	4	2	16	16	400	3.00	2.46	1.80	0.90
							16-3	0.46	5	5	8	8	420	1.92	1.70	1.60	0.78
							16-4	0.91	6	3	6	5	400	2.00	1.38	1.22	0.52
							16-5	1.11	20	16	3	2	540	3.00	2.82	2.16	0.70
17	0	0	0	0.51	0.50	0.51	17-1	1.31	7	3	5	2	430	2.34	1.76	1.50	0.54
							17-2	1.25	11	6	1	1	660	2.82	2.60	2.00	0.74
							17-3	1.34	8	3	1	0	490	2.20	1.54	1.24	0.74
							17-4	1.24	10	4	5	3	400	2.00	1.74	1.32	0.50
							17-5	1.58	13	8	2	1	520	2.54	2.18	1.46	0.62

The mean ± standard deviation of N_1, N_2, L, D_{S1}, D_{d1}, D_{d2}, and D_{s2} were 9.27 ± 4.75, 7.35 ± 4.49, 480.71 ± 71.01, 2.60 ± 0.49, 2.18 ± 0.44, 1.61 ± 0.33, and 0.73 ± 0.20 mm, respectively. Table 4 summarizes the experimental and statistical results.

Correlation Analysis between the Maximum Singular Value and Other Parameters

Using SPSS software (IBM SPSS 27.0, Chicago, IL, USA), multiple linear regression analysis was conducted with the MSV as the dependent variable. The excitation parameters (X_1, X_2, and X_3), response outcomes (Y_1, Y_2, and Y_3), and branch morphological parameters (L, D_{S1}, D_{d1}, D_{d2}, and D_{s2}) were treated as independent variables. Figure 4 shows the Pearson correlation heatmap. The correlation coefficients between the MSV and branch morphological parameters (L, D_{S1}, D_{d1}, D_{d2}, and D_{s2}) were all less than or equal to the absolute value of 0.125, indicating extremely weak or negligible linear correlations.

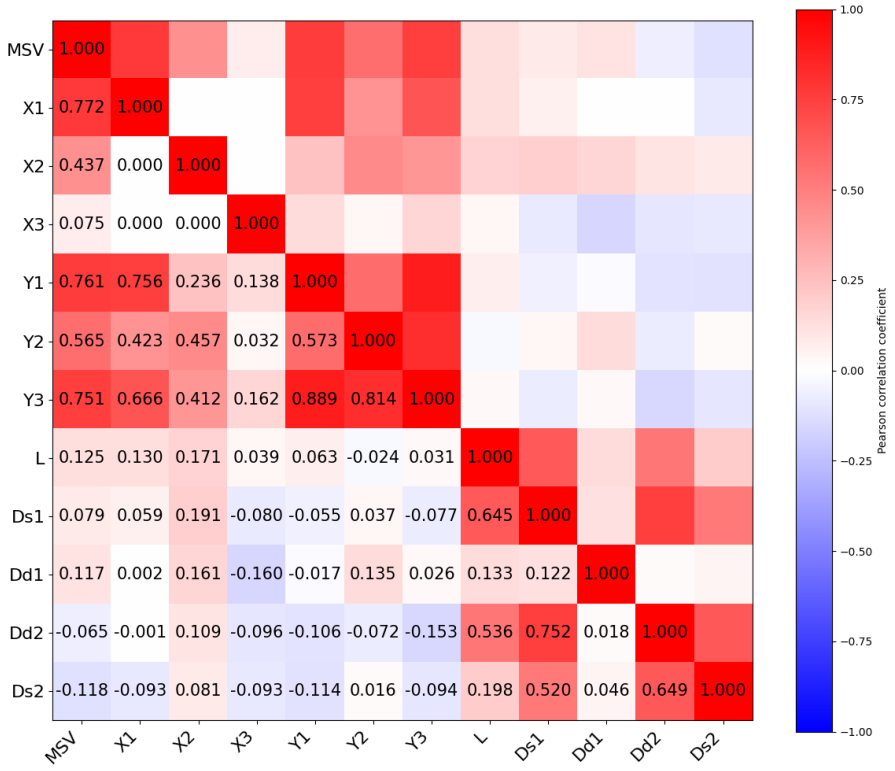

Fig. 4. Pearson correlation coefficients among maximum singular value, excitation parameters, response outcomes, and branch morphological parameters

In contrast, the fruit detachment percentages exhibited stronger correlations with the MSV. The Pearson correlation coefficients of Y_1, Y_2, and Y_3 with the MSV were 0.761, 0.565, and 0.751, respectively, indicating the strong positive linear relationship of the MSV with Y_1 and Y_3. This suggests that increases in the MSV correspond to a synchronous increase in these detachment percentages. The Y_2 had a moderate positive correlation with the MSV but a weaker association compared with Y_1 and Y_3. These results demonstrate a strong positive relationship between the branch vibration state and harvesting performance, suggesting that the MSV can serve as an indicator of wolfberry harvesting efficiency and can be used to optimize excitation parameters during non-harvest periods or in simulation environments.

Regarding the excitation parameters, the linear correlation coefficients of X_1, X_2, and X_3 with the MSV were 0.772, 0.437, and 0.075, respectively, indicating that the amplitude of the excitation had a moderate positive effect on the MSV, that the secondary amplitude had a weak positive effect, and that the phase had a negligible negative effect. This shows that excitation amplitude has a more significant impact on the MSV than the excitation phase. Significant correlations were observed between excitation parameters (X_1, X_2, and X_3) and response outcomes (Y_1, Y_2, and Y_3), which were further quantitatively analyzed using RSM (Section of Multiple Regression Analysis of Excitation Parameters).

Singular Value Spectrum Analysis

The upper curve represents the first singular value, corresponding to the component with the strongest energy at each frequency and reflecting the true physical mode of the system, *i.e.*, the natural frequency. The lower curve represents the second singular value, corresponding to the next-strongest energy component, which is typically associated with noise, computational modes, or closely spaced modes. Using test 14-2 in Table 4 as an example, Fig. 5(a) shows that the first singular value exhibited a peak near 4 Hz (MSV approximately 2.15) and a smaller secondary peak near 8 Hz, indicating the presence of two separable modes. For wolfberry branches measured with a two-channel setup, the primary modal energy in low-order modes was concentrated in the first singular value. The peak frequency of the first singular value in the singular value spectrum is a key indicator for identifying the branch's natural frequency. If the second singular value exhibits a peak coinciding with the first singular value peak or an independent secondary peak with significant energy, then it can be used to validate the natural frequency location. Figures 5(b) and 5(c), showing amplitude–frequency plots for the upper and lower acceleration sensors (UAS and LAS), display clear peaks near 4 Hz and 8 Hz, thereby improving the reliability of natural frequency identification. These two low-order modal frequencies are similar to the results reported by Su *et al.* (2025). An excitation frequency of 4 Hz almost coincides with the first natural frequency, producing a "quasi-resonance" effect, indicating that a relatively large vibration response can be achieved with minimal input energy under appropriate vibration frequency, phase, and location conditions. As shown in Fig. 5(a), the first singular value decreases sharply after the 4 Hz peak and drops to only 23.95% of the maximum value by 8 Hz, indicating substantial damping in the branch. Figures 5(b) and 5(c) show that the 4 Hz peak has a notable width, rather than a sharp "needle-like" spike, confirming the presence of damping, consistent with the findings of So (2003).

A notable difference was observed between the amplitude–frequency spectra of the upper and lower acceleration sensors. The spectrum from the LAS (Fig. 5(c)) was visibly smoother and simpler than that from the UAS (Fig. 5(b)), with the minor spectral features largely absent and only the dominant peaks near 4 Hz and 8 Hz remaining prominent. This phenomenon can be attributed to the frequency-dependent attenuation characteristics of the wolfberry branch as a viscoelastic biomaterial. As vibration energy propagates along the branch toward the distal (lower) region, higher-frequency components and minor vibrational modes are preferentially dissipated because the damping coefficient of plant tissues generally increases with frequency. As a result, by the time the vibration signal reaches the lower sensor position, the minor modes have largely dissipated, leaving a smoother spectrum dominated by the fundamental mode near 4 Hz. This phenomenon is consistent with the high damping characteristics revealed by the singular value spectrum analysis and the energy attenuation behavior documented in previous studies (He *et al*. 2018; Sola-Guirado *et al*. 2022).

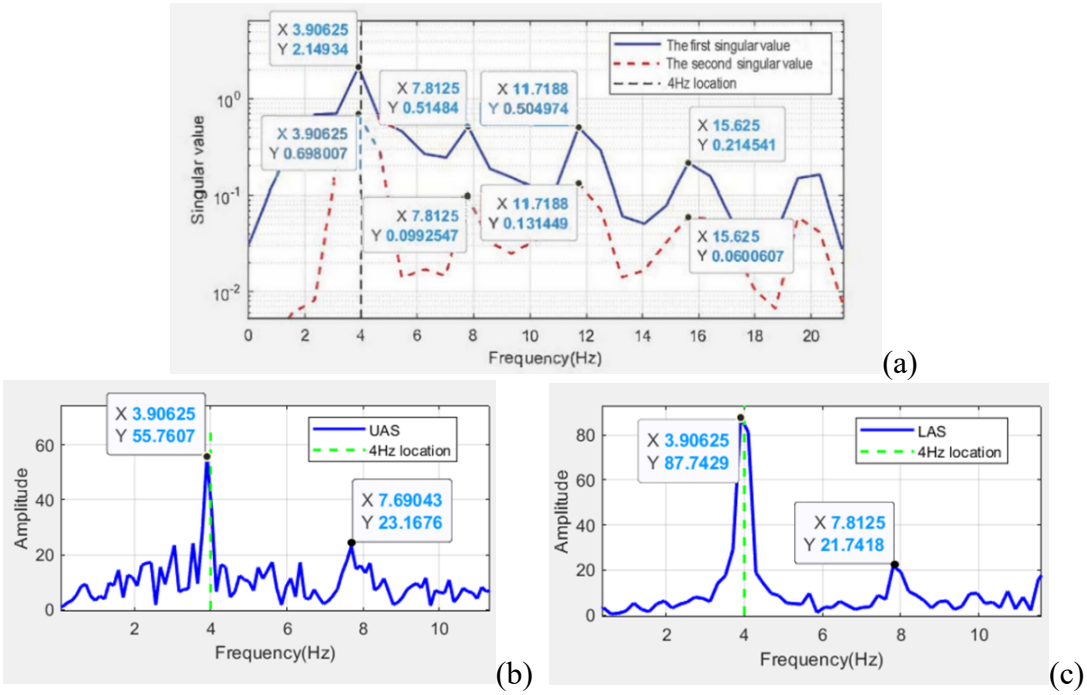

Fig. 5. Acceleration signal processing results for test 14-2: (a) singular value spectrum, (b) amplitude–frequency plot of the upper acceleration sensor, and (c) amplitude–frequency plot of the lower acceleration sensor

Multiple Regression Analysis of Excitation Parameters

Response surface analysis of DPM (Y_1)

Table 5 reports the analysis of variance (ANOVA) results used to generate the quadratic model. X_1, X_2, X_3, X_1X_2, and X_2X_3 had significant effects ($P < 0.05$) on the DPM. The coefficients of the DPM model responses using the factor codes as variables were expressed as follows:

$$Y_1 = 0.50 + 0.32X_1 + 0.10X_2 + 0.09X_3 - 0.09X_1X_2 + 0.01X_1X_3 + 0.08X_2X_3 + 0.04X_1^2 - 0.07X_2^2 - 0.05X_3^2 \quad (12)$$

Table 5. ANOVA Results of the Quadratic Model Response to DPM

Items	Sum of Squares	DOF	Mean Square	F-value	P-value
Model	1.08	9	0.1200	29.60	< 0.0001***
X_1	0.8405	1	0.8405	207.22	< 0.0001***
X_2	0.0821	1	0.0821	20.23	0.0028**
X_3	0.0654	1	0.0654	16.11	0.0051**
X_1 X_2	0.0299	1	0.0299	7.37	0.0300*
X_1 X_3	0.0004	1	0.0004	0.1071	0.7530
X_2 X_3	0.0267	1	0.0267	6.57	0.0373*
X_1^2	0.0052	1	0.0052	1.28	0.2956
X_2^2	0.0216	1	0.0216	5.34	0.0542
X_3^2	0.0088	1	0.0088	2.18	0.1836
Residual	0.0284	7	0.0041		
Lack of fit	0.0132	3	0.0044	1.17	0.4265
Pure error	0.0151	4	0.0038		

Note: *(P<0.05): Significant difference; **(P<0.01): The difference is very significant; ***(P<0.001): The difference is highly significant. The same below.

RSM was used to analyze the interactive effects of the amplitudes of the UVS and LVS and the excitation phase on DPM. As shown in Fig. 6(a), the interaction between the amplitudes of the UVS and LVS had a significant effect on DPM. When the excitation phase was zero and the LVS amplitude was high, DPM initially increased and then decreased with the increasing UVS amplitude. Figure 6(c) shows that when the UVS amplitude was zero, there was an interactive effect of the excitation phase and LVS amplitude on DPM. Specifically, when the excitation phase was low, DPM first increased and then decreased as the LVS amplitude increased. The middle section of the branch was subjected to the combined excitation of the UVS and LVS, achieving a superimposed vibration state. Changes in the amplitudes of the UVS and LVS and excitation phase altered the branch vibration mode. When the branch vibration pattern resembled a specific modal shape, it resulted in intense vibration, which was reflected by higher MSVs and increased fruit detachment percentages. Figure 6(b) shows that when the LVS amplitude was zero, DPM decreased as the UVS amplitude and excitation phase decreased. The influence of the UVS amplitude on DPM was slightly greater than that of the excitation phase.

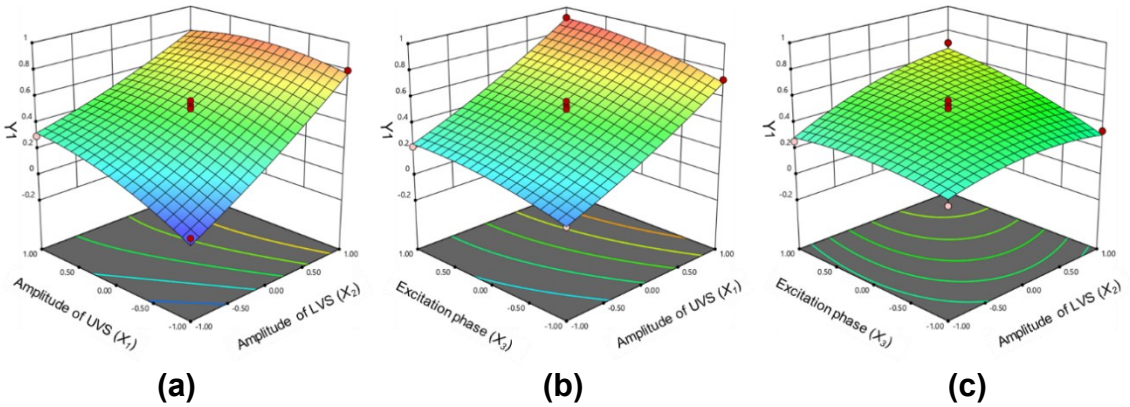

(a) (b) (c)

Fig. 6. Response surfaces of the effects of interactive factors on DPM

Response surface analysis of DPL

Table 6 shows the ANOVA results used to determine the quadratic model. X_1, X_2, and X_1X_2 exhibited significant effects ($P < 0.05$) on the multiples index.

Table 6. ANOVA Results of the Quadratic Model Response to DPL

Items	Sum of Squares	DOF	Mean Square	F-value	P-value
Model	1.06	9	0.1180	9.17	0.0040**
X_1	0.4035	1	0.4035	31.35	0.0008***
X_2	0.4796	1	0.4796	37.26	0.0005***
X_3	0.0013	1	0.0013	0.1035	0.7570
$X_1 X_2$	0.0815	1	0.0815	6.33	0.0400*
$X_1 X_3$	0.0001	1	0.0001	0.0056	0.9424
$X_2 X_3$	0.0023	1	0.0023	0.1765	0.6870
X_1^2	0.0013	1	0.0013	0.1026	0.7581
X_2^2	0.0436	1	0.0436	3.39	0.1082
X_3^2	0.0418	1	0.0418	3.25	0.1146
Residual	0.0901	7	0.0129		
Lack of fit	0.0546	3	0.0182	2.05	0.2493
Pure error	0.0355	4	0.0089		

The coefficients of DPL model responses (Y_2) using the factor codes as variables were expressed as follows:

$$Y_2 = 0.63 + 0.22X_1 + 0.24X_2 + 0.01X_3 - 0.14X_1X_2 + 0.02X_2X_3 + 0.02X_1^2 - 0.10X_2^2 - 0.10X_3^2 \quad (13)$$

As shown in Fig. 7(a), the interaction between the UVS and LVS amplitudes had a significant effect on DPL. The lowest DPL was observed when both the UVS and LVS amplitudes were at low levels. According to Fig. 7(b), for a given excitation phase, DPL increased rapidly with an increasing UVS amplitude. Figure 7(c) shows that the variation in DPL considering the LVS amplitude was similar to the trend observed in Fig. 6(b) for DPL considering the UVS amplitude.

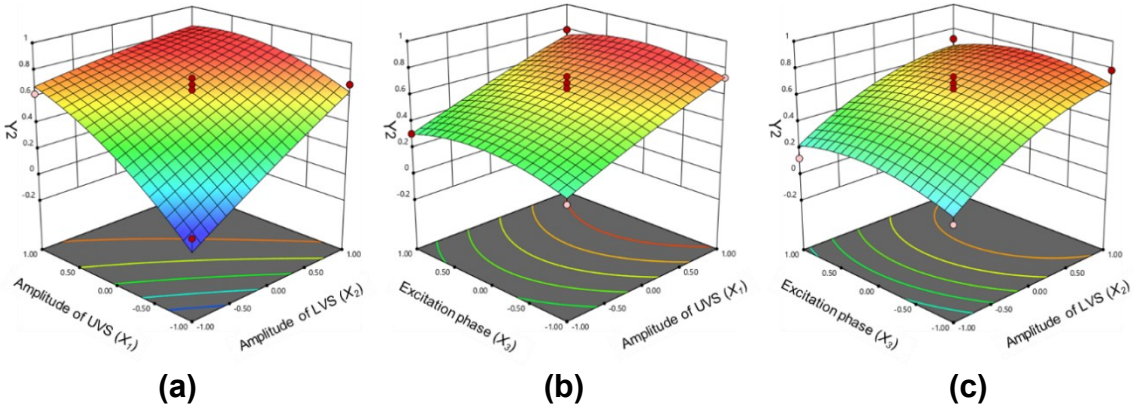

Fig. 7. Response surfaces of the effects of interactive factors on DPL

Response Surface Analysis of TD

Table 7 reports the ANOVA results used to determine the quadratic model. X_1, X_2, X_3, X_1X_2, X_2^2, and X_3^2 had significant effects ($P < 0.05$) on TD. The coefficients of the TDR model responses (Y_3) using the factor codes as variables were expressed as follows:

$$Y_3 = 0.56 + 0.27X_1 + 0.16X_2 + 0.06X_3 - 0.12X_1X_2 + 0.04X_2X_3 + 0.02X_1^2 - 0.08X_2^2 - 0.07X_3^2 \quad (14)$$

Table 7. ANOVA Results of the Quadratic Model Response to TD

Items	Sum of Squares	DOF	Mean Square	F-value	P-value
Model	0.9652	9	0.1072	27.14	0.0001***
X_1	0.6009	1	0.6009	152.08	< 0.0001***
X_2	0.2158	1	0.2158	54.61	0.0002***
X_3	0.0288	1	0.0288	7.28	0.0307*
X_1 X_2	0.0560	1	0.0560	14.17	0.0070***
X_1 X_3	0.0001	1	0.0001	0.0145	0.9075
X_2 X_3	0.0071	1	0.0071	1.79	0.2231
X_1^2	0.0019	1	0.0019	0.4850	0.5086
X_2^2	0.0301	1	0.0301	7.61	0.0282*
X_3^2	0.0229	1	0.0229	5.80	0.0469*
Residual	0.0277	7	0.0040		
Lack of fit	0.0203	3	0.0068	3.67	0.1208
Pure error	0.0074	4	0.0018		

For TD, the UVS and LVS amplitudes exhibited an interactive effect. As shown in Fig. 8(a), when the excitation phase was zero, TD increased with the LVS amplitude for a given UVS amplitude, and this increasing trend was more pronounced when the UVS amplitude was lower. When the LVS amplitude was high, changes in TDR with varying UVS amplitudes were relatively small, remaining at high values. Furthermore, as shown in Figs. 8(b) and 8(c), TD reached its maximum when the excitation phase was high and both the LVS and UVS amplitudes were high.

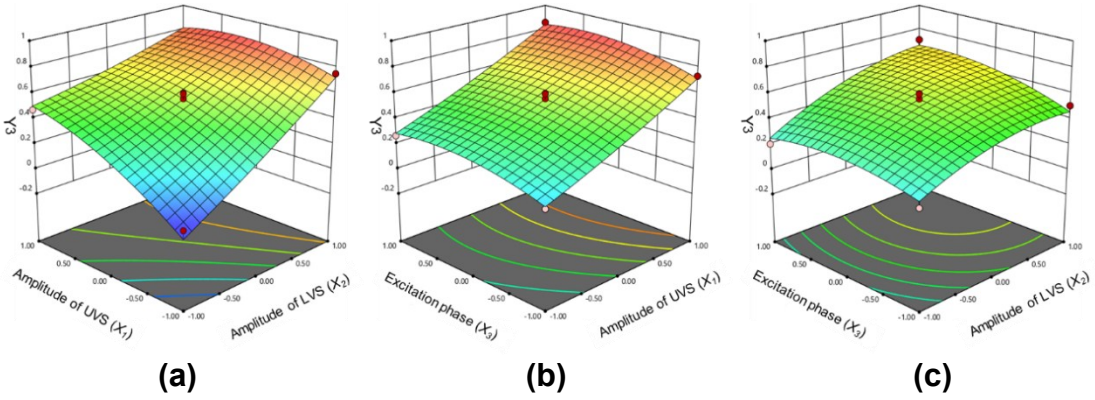

Fig. 8. Response surfaces of the effects of interactive factors on TD

Optimization analysis and experimental validation

To achieve optimal harvesting performance, parameter optimization was conducted using Design-Expert 13.0 software with factors X_1, X_2, and X_3 and the objectives of maximizing DPM (Y_1), DPL (Y_2), and TD (Y_3). The predicted optimal results showed a DPM of 0.920, DPL of 0.804, and TD of 0.868 when the UVS amplitude, LVS amplitude, and excitation phase were set at 79.43 mm, 67.39 mm, and 137.16°, respectively. Based on these optimized parameters, experimental trials were conducted with five replicates, the results of which are summarized in Table 8. The experimental outcomes were closely matched with the predicted values with relative deviations of 6.20% for DPM, 5.97% for DPL, and 1.04% for TD. A TD of 85.9% demonstrated acceptable harvesting performance under low-frequency vibration conditions, which is comparable to the harvesting percentages reported in recent studies (Chen *et al.* 2024a; Mei *et al.* 2024; Wei *et al*. 2025). The vibration frequency remains a critical factor influencing wolfberry fruit detachment.

Table 8. Comparison of the Simulation Test and Experimental Results

	Amplitude of UVS (mm)	Amplitude of LVS (mm)	Excitation phase (°)	DPM	DPL	TD
Predicted results	79.43	67.39	137.16	0.920	0.804	0.868
Experimental results	80	68	135	0.863	0.852	0.859

LIMITATIONS AND FUTURE RESEARCH

This study supports the feasibility of dual-point cooperative excitation for overcoming energy attenuation and improving low-frequency harvesting efficiency. The

application of singular value spectrum analysis to wolfberry harvesting research provides a significant methodological tool for understanding the dynamics of the branch–fruit system and enabling precise control based on vibration state feedback. Future research should build upon this foundation to explore multi-source configuration strategies and the effects of higher-frequency excitation (within damage thresholds) to further enhance the harvesting performance.

Although the excitation frequency was fixed at 4 Hz in this study due to the operational limit of the DC motor, the singular value spectrum analysis revealed a second dominant mode near 8 Hz, suggesting the potential benefit of exploring higher excitation frequencies. Future research should employ excitation devices capable of reaching higher frequencies (*e.g*., 4 to 10 Hz) to investigate whether excitation at or near the second modal frequency can further enhance fruit detachment. Moreover, the simultaneous application of two different excitation frequencies (*e.g*., 4 Hz and 8 Hz) through the upper and lower vibration sources represents a particularly promising direction.

Conducting experiments on cut branches leads to progressive moisture loss from the branch tissue. The resulting decrease in branch moisture content may alter the viscoelastic properties of the branch tissue, the fruit-pedicel abscission force, and the damping characteristics of the branch–fruit system. Although each branch in this study was tested within approximately 20 minutes of cutting, this cannot fully replicate the physiological conditions of an intact plant. Furthermore, variations in environmental conditions (*e.g*., temperature, humidity, and wind speed) over the 4-day field experimental period may have increased the scatter in the experimental results. Therefore, the regression coefficients and optimal parameter values reported in this paper are applicable only to the tested experimental conditions, and their direct application to the harvesting of intact plants requires further validation.

This study focused exclusively on fruit detachment percentages and did not quantify fruit damage. During the experiments, observations suggested that visible mechanical damage to ripe berries was minimal under the low-frequency (4 Hz) excitation conditions, likely because the lower inertial forces associated with low-frequency vibration are inherently gentler than those generated by higher-frequency methods (*e.g*., 15 to 48 Hz) reported in previous studies (Deng *et al.* 2026). Nevertheless, the absence of quantitative damage data (such as the percentage of bruised, cracked, or juice-leaking berries) represents a limitation. Additionally, the detachment of unripe fruit, which is an important quality indicator for wolfberry harvesting, was not assessed in this study. Future work should incorporate damage classification and unripe fruit detachment measurements alongside detachment percentage analyses to provide a evaluation of harvesting quality under dual-source excitation.

It should be noted that the regression models and optimal parameters identified in this study are specific to the ‘Ningqi No. 7’ cultivar tested under the particular growing conditions of the experimental orchard. Biological variability (including differences in ripeness stage, berry size and weight, branch thickness, stiffness, and moisture content) would inevitably affect the specific regression coefficients if the experiments were repeated with different plant material or under different environmental conditions. Subtle differences in growing conditions, plant maturity, or cultivar characteristics could alter branch mechanical properties and fruit–pedicel abscission force, thereby shifting the quantitative relationships. Therefore, the specific regression equations should be regarded as applicable within the scope of the tested conditions rather than as universally predictive models. Nevertheless, the fundamental finding that dual-source excitation with controlled

amplitude and phase enhances branch vibration energy (as quantified by MSV) and promotes fruit detachment is expected to remain valid across conditions, as it is rooted in the basic vibration mechanics of the branch–fruit system. Future studies should validate the proposed methodology across multiple cultivars, ripeness stages, and growing environments to establish its broader applicability.

CONCLUSIONS

This study systematically investigated the vibration harvesting mechanism and parameter optimization of wolfberry (*Lycium barbarum* L.) branches using dual-source excitation experiments and singular value spectrum analysis. The main conclusions are as follows:

1. The low-frequency vibration modes and high damping characteristics of wolfberry branches were revealed. Singular value spectrum analysis identified two dominant low-frequency modes near 4 and 8 Hz in the 0 to 25 Hz range for the tested branches. The broad, blunt peaks and rapid energy decay of the singular value curves confirmed the high structural damping inherent to the branches as a biomaterial. This explains the rationale and necessity for employing low-frequency excitation and provides a basis for avoiding potential damage caused by high-frequency vibrations.
2. A quantitative relationship between the branch vibration state and harvesting effectiveness was established. This study found that the maximum singular value (MSV), which represents the overall vibration energy of the branch, exhibited strong positive linear correlations with both total detachment percent (TD) and detachment percentage in the middle (DPM), with correlation coefficients of 0.751 and 0.761, respectively. This establishes a pathway linking: excitation parameters → vibration state (MSV) → harvesting effectiveness. Consequently, the MSV can serve as a reliable physical indicator for the rapid prediction and optimization of excitation parameters during non-harvesting periods or in simulation environments.
3. The patterns of dual-source excitation parameters were characterized, and the optimal combination was determined. RSM indicated that the UVS and LVS amplitudes had a highly significant positive effect on the detachment percentage. The influence of the excitation phase was more complex, affecting vibration patterns *via* its interaction with amplitude. With the excitation frequency fixed at 4 Hz, which is close to the first-order natural frequency of wolfberry branches, optimization of the amplitude and phase combination induced a more intense quasi-resonant response in the branch. The optimal parameter combination was identified as a UVS amplitude of 80 mm, LVS amplitude of 68 mm, and an excitation phase of 135°. Validation tests under these parameters achieved a TDR of 85.9%, validating the effectiveness of the optimization.

ACKNOWLEDGMENTS

The authors are grateful for the support of Key Research and Development Project of Ningxia Hui Autonomous Region (2024BEH04137), Natural Science Foundation of Ningxia (2025AAC030073), and North Minzu University (2021KYQD31). We thank

LetPub (www.letpub.com.cn) for its linguistic assistance during the preparation of this manuscript.

REFERENCES CITED

Bu, L., Hu, G., Chen, C., Sugirbay, A., and Chen, J. (2020). "Experimental and simulation analysis of optimum picking patterns for robotic apple harvesting," *Scientia Horticulturae* 261, article ID 108937. https://doi.org/10.1016/j.scienta.2019.108937

Chen, Q., Kang, R., Wei, N., Fan, Y., Wang, Z., Chen, Y., and Chen, J. (2024a). "Design and experiment optimize of the vibration harvesting machine of *Lycium barbarum* L," *Journal of Agricultural Engineering* 55(4), article 1597. https://doi.org/10.4081/jae.2024.1597

Chen, Q., Zhang, S., Wei, N., Li, P., Hu, G., Chen, J., and Chen, Y. (2024b). "Design and optimization of torsion harvester of *Lycium barbarum* L," *International Journal of Agricultural and Biological Engineering* 17(4), 109-115. https://doi.org/10.25165/j.ijabe.20241704.8082

Chen, Q., Zhang, S., Wei, N., Fan, Y., Zhang, W., Wang, Z., Chen, J., and Chen, Y. (2025a). "Optimizing the parameters for the vibration harvesting of *Lycium barbarum* L. under various excitation modes," *Transactions of the Chinese Society of Agricultural Engineering* 41(3), 32-42. https://doi.org/10.11975/j.issn.1002-6819.202408110

Chen, Q., Wei, N., Fan, Y., Wang, Z., Zhou, J., Gao, Z., Chen, Y., and Chen, J. (2025b) "Fruit-flower-leaf dynamic response of *Lycium barbarum* L. for vibration harvesting," S*mart Agricultural Technology* 10, article ID 100722. https://doi.org/10.1016/j.atech.2024.100722

Chen, Y., Zhao, J., Hu, G., and Chen, J. (2021). "Design and testing of a pneumatic oscillating Chinese wolfberry harvester," *Horticulturae* 7(8), article 214. https://doi.org/10.3390/horticulturae7080214

Deng, B., Wang, X., Wang, K., Song, H., Gao, S., Tu, Y., and Zhang, X. (2025). "Analysis of energy transfer characteristics in multi-level branches of *Lycium barbarum* L. under vibration excitation," *Computers and Electronics in Agriculture* 239, article ID 110992. https://doi.org/10.1016/j.compag.2025.110992

Deng, B., Wang, X., Zhang, X., Xu, J., and Tu, Y. (2026). "Current status and future trends in mechanized harvesting systems for wolfberry (*Lycium barbarum* L.)," *Revista Brasileira de Engenharia Agrícola e Ambiental* 30(3), article ID e291574. https://doi.org/10.1590/1807-1929/agriambi.v30n3e291574

He, M., Kan, Z., Li, C., Wang, L., Yang, L., and Chen, X. (2018). "Study on the dynamic characteristics of *Lycium Barbarum* plant," *Journal of Agricultural Mechanization Research* 40(5), 18-23. https://doi.org/10.13427/j.cnki.njyi.2018.05.003

Jiang, Y., Han, C., Guo, J., and Ma, J. (2024). "Structure design and modeling simulation analysis of flexible brush type wolfberry harvesting machinery," *Journal of Anhui Agricultural Sciences* 52(12), 192-196, 221. https://doi.org/10.3969/j.issn.0517-6611.2024.12.040

Klema, V., and Laub, A. (1980). "The singular value decomposition: Its computation and some applications," *IEEE Transactions on Automatic Control* 25(2), 164-176. https://doi.org/10.1109/TAC.1980.1102314

Li, Y., Hu, Z., Zhang, Y., Wang, J., and Xu, J. (2024). "Research progress of technology and equipment for mechanized harvest of wolfberry," *Journal of Chinese Agricultural Mechanization* 45(5), 16-21, 45. https://doi.org/10.13733/j.jcam.issn.2095-5553.2024.05.003

Liu, M., Zhang, Y., Li, Z., Chen, J., and Yin, G. (2017). "Application of singular value energy standard spectrum in noise reduction of mechanical vibration signal," *Mechanical Science and Technology for Aerospace Engineering* 36(1), 46-51.

Macoretta, G., Luglio, S., Conforti, F., Abruzzo, M., Gagliardi, L., Fontanelli, M., and Raffaelli, M. (2025). "Analysis of olive detachment force to improve olive shaker efficiency through branch modeling," *AgriEngineering* 7(2), article 28. https://doi.org/10.3390/agriengineering7020028

Malchaire, J., Rodriguez, Diaz., Piette, A., Gonçalves, A., and de Schaetzen, D. (1998). "Neurological and functional effects of short-term exposure to hand-arm vibration," *International Archives of Occupational and Environmental Health* 71(4), 270-276. https://doi.org/10.1007/s004200050280

Mei, S., Tang, D., Shi, Z., Song, Z., Tian, Z., and Zhou, R. (2024). "Design and test of a Chinese wolfberry harvester using arrayed vibration units," *Transactions of the Chinese Society of Agricultural Engineering* 40(23), 115-125. https://doi.org/10.11975/j.issn.1002-6819.202407252

Mei, S., Xiao, H., Shi, Z., Jiang, Q., Zhao, Y., and Ding, W. (2019). "Design and test of low-loss *Lycium barbarum* harvesting technology and equipment based on reciprocating vibration method," *Journal of Chinese Agricultural Mechanization* 40(11), 100-105, 208. https://doi.org/10.13733/j.jcam.issn.2095-5553.2019.11.16

Miao, Y., Zhong, M., Liu, Z., and Sun, F. (2015). "Analysis of wood vibration energy attenuation based on FFT vibration signal," *BioResources* 10(1), 272-281. https://doi.org/10.15376/biores.10.1.272-281

Morioka, M., and Griffin, M. (2002). "Dependence of vibrotactile thresholds on the psychophysical measurement method," *International Archives of Occupational and Environmental Health* 75(1), 78-84. https://doi.org/10.1007/s004200100280

Peng, Y., Zhang, Z., Liu, Y., Xu, T., Zhang, L., and Wang, R. (2019). "Kinematics and vibration mode analysis of vibrating harvesting for wolfberry," *Mechanical Research and Application* 32(2), 8-13, 16. https://doi.org/10.16576/j.cnki.1007-4414.2019.02.04

So, J. (2003). "Vibratory harvesting machine of boxthorn (*Lycium chinense* Mill) berries," *Transactions of the ASAE* 46(2), 211-221. https://doi.org/10.13031/2013.12963

Sola-Guirado, R., Luque-Mohedano, R., Tombesi, F., and Blanco-Roldan, G. (2022). "Effect of leaves in the dynamic response of olive tree branches and their computational model," *Computers and Electronics in Agriculture* 203, article ID 107490. https://doi.org/10.1016/j.compag.2022.107490

Su, X., Liu, Y., Liu, J., and Zhao, D. (2025). "Experiment and analysis of vibration response in fruit-bearing branches of wolfberry," *Scientia Silvae Sinicae* 61(8), 25-31. https://doi.org/10.11707/j.1001−7488.LYKX20240470

Wall, M., Rechtsteiner, A., and Rocha, L. (2003). "Singular value decomposition and principal component analysis," in: *A Practical Approach to Microarray Data Analysis*, Springer, 91-109. https://doi.org/10.1007/0-306-47815-3_5

Wan, F., Sun, H., Du, X., Li, S., Zhao, Y., and Huang, X. (2021). "Design and test of self-propelled *Lycium barbarum* vibrating harvester," *Agricultural Research in the Arid Areas* 39(5), 231-238. https://doi.org/10.7606/j.issn.1000-7601.2021.05.30

Wang, Y., Chen, Y., Han, B., and Chen, J. (2018). "Research on laws of wolfberry dropping based on high-speed camera," *Journal of Agricultural Mechanization Research* 40(11), 166-170. https://doi.org/10.13427/j.cnki.njyi.2018.11.031

Wei, N., Chen, Q., Zhang, D., Fan, Y., Zhang, W., Wen, S., Chen, J, Bu, L., and Mei, S. (2025). "Design and experimental optimization of a continuous vibration based *Lycium barbarum* L. harvesting device," *INMATEH-Agricultural Engineering* 77(3), 689-701. https://doi.org/10.35633/inmateh-77-56

Zhang, W., Zhang, M., Zhang, J., and Li, W. (2018). "Design and experiment of vibrating wolfberry harvester," *Transactions of the Chinese Society for Agricultural Machinery* 49(7), 97-102. https://doi.org/10.6041/j.issn.1000-1298.2018.07.012

Zhang, Z., Xiao, H., Ding, W., and Mei, S. (2015). "Mechanism simulation analysis and prototype experiment of *Lycium barbarum* harvest by vibration mode," *Transactions of the Chinese Society of Agricultural Engineering* 31(10), 20-28. https://doi.org/10.11975/j.issn.1002-6819.2015.10.003

Zhao, J., Ma, T., Inagaki, T., Chen, Y., Hu, G., Wang, Z., Chen, Q., Gao, Z., Zhou, J., Wang, M., Tsuchikawa, S., and Chen, J. (2021a). "Parameter optimization of vibrating and comb-brushing harvesting of *Lycium barbarum* L. based on FEM and RSM," *Horticulturae* 7(9), article 286. https://doi.org/10.3390/horticulturae7090286

Zhao, J., Tsuchikawa, S., Ma, T., Hu, G., Chen, Y., Wang, Z., Chen, Q., Gao, Z., and Chen, J. (2021b). "Modal analysis and experiment of a *Lycium barbarum* L. shrub for efficient vibration harvesting of fruit," *Agriculture* 11(6), article 519. https://doi.org/10.3390/agriculture11060519

Article submitted: February 4, 2026; Peer review completed: February 28, 2026; Revised version received: March 2, 206; Accepted: March 4, 2026; Published: March 13, 2026.
DOI: 10.15376/biores.21.2.3931-3953